New angles on top quark decay to a charged Higgs

View the article online for updates and enhancements.

New angles on top quark decay to a charged Higgs

David Eriksson, Gunnar Ingelman, Johan Rathsman and Oscar Stål[*]

High-Energy Physics, Department of Nuclear and Particle Physics,
Uppsala University, P. O. Box 535, SE-751 21 Uppsala, Sweden
E-mail: `david.eriksson@tsl.uu.se`, `gunnar.ingelman@tsl.uu.se`,
`johan.rathsman@tsl.uu.se`, `oscar.stal@tsl.uu.se`

ABSTRACT: To properly discover a charged Higgs Boson ($H^{\pm}$) requires its spin and couplings to be determined. We investigate how to utilize $t\bar{t}$ spin correlations to analyze the $H^{\pm}$ couplings in the decay $t \to bH^+ \to b\tau^+\nu_\tau$. Within the framework of a general Two-Higgs-Doublet Model, we obtain results on the spin analyzing coefficients for this decay and study in detail its spin phenomenology, focusing on the limits of large and small values for $\tan\beta$. Using a Monte Carlo approach to simulate full hadron-level events, we evaluate systematically how the $H^{\pm} \to \tau^{\pm}\nu_\tau$ decay mode can be used for spin analysis. The most promising observables are obtained from azimuthal angle correlations in the transverse rest frames of $t(\bar{t})$. This method is particularly useful for determining the coupling structure of $H^{\pm}$ in the large $\tan\beta$ limit, where differences from the SM are most significant.

KEYWORDS: Spin and Polarization Effects, Higgs Physics, Beyond Standard Model, Hadronic Colliders.

[*]Corresponding author

Contents

1. Introduction

Finding a fundamental spin zero boson with electric charge would be a direct sign of physics beyond the Standard Model (SM). The existence of a charged Higgs boson pair ($H^{\pm}$) with these properties is predicted by Two-Higgs-Doublet Model (2HDM) extensions of the SM Higgs sector. The primary motivation for studying the 2HDM is supersymmetry, which requires an even number of Higgs doublets for cancellation of triangle anomalies. Charged Higgs searches at hadron colliders are divided into two regimes, separated by the dominant mode of production. When $H^{\pm}$ is heavy ($m_{H^+} \gtrsim m_t$), it is produced primarily through the $gg \rightarrow H^+ \bar{t} b$ and $gb \rightarrow H^+ \bar{t}$ processes [1–4]. When, on the other hand, $H^{\pm}$ is light ($m_{H^+} < m_t - m_b$) and the decay $t \rightarrow bH^+$ [5–9] opens up, this quickly becomes the dominant production mode.

The most stringent model-independent limit on the mass of $H^{\pm}$ from a direct search experiment comes from LEP: $m_{H^+} > 79.3\,\text{GeV}$ [10] at 95% CL, assuming only the decays $H^+ \rightarrow c\bar{s}$ and $H^+ \rightarrow \tau^+ \nu_{\tau}$ are possible. Even tighter constraints on m_{H^+} have later been derived using Tevatron data [11], but these are not independent of the other 2HDM parameters. Neither are indirect constraints on m_{H^+} obtained from B-physics observables.

The upcoming searches for $H^\pm$ planned by the LHC experiments will have good sensitivity to discover $H^\pm$ over a wide parameter range [12−16], especially when $H^\pm$ is light. However, even if some candidate $H^\pm$ state was to be found, this discovery alone would not be enough to establish the validity of the Higgs mechanism as described by the 2HDM. To do this requires further that the spin, and the couplings, of this new particle be determined. Here we investigate one possibility to address this issue when $m_{H^+} < m_t - m_b$. In addition to providing a discovery channel, the $t \to bH^+$ decay mode could modify the ordinary V-A Lorentz structure of weak top decay significantly. As we will show, this fact can provide a handle on the spin and coupling structure of $H^\pm$ by making use of spin correlations.

Top quarks produced in pairs at hadron colliders constitute an interesting laboratory for observing spin effects in high-energy physics. Since the timescale for weak top decay $1/\Gamma_t$ is much shorter than the typical hadronization timescale $1/\Lambda_{\mathrm{QCD}}$, the heavy quarks will decay before hadrons can form [17]. No hadronic effects will therefore obfuscate the spin information. Unlike the case for the lighter quarks, this fact allows for reliable perturbative calculations of the relevant spin observables. Furthermore, since the charged current weak interaction violates parity maximally, the decay self-analyzes the spin of the top quark. This means the full spin information will be imprinted in the angular distributions of the different decay products.

In order for the angular information to be useful for investigating the couplings involved, a method to determine the spin projection of the decaying top quark is required. At a hadron collider, this can be achieved by exploiting *correlations* between the top quark spins. By using the decay information from one side of a $t\bar{t}$ event, it is possible to determine statistically the polarization of the other top. Spin correlations in top quark pair production and decay have been extensively discussed within the Standard Model (SM) for hadron-hadron colliders [18−30], and for e^+e^- experiments [31−36]. Utilizing the top spin information to study physics beyond the Standard Model was considered in the context of anomalous Wtb-couplings [31, 37, 38], for probing extended Higgs sectors and effects of CP-violation [39−44] , and within theories with extra dimensions [45, 46].

We study the spin phenomenology of a light scalar sector in full generality, ignoring indirect constraints on the 2HDM. We will however restrict the mass to $m_{H^+} \gtrsim m_W$, as required by the non-observation of $H^\pm$ in direct search experiments. Due to the, in the context of spin observables, relatively limited sample of $t\bar{t}$ events available from the Tevatron, our main focus will be on prospects for observations at the LHC. We try to comment on issues that are of relevance also for the analysis of Tevatron data.

The organization of this paper is as follows. First, in section 2, we discuss $t\bar{t}$ pair production at hadron colliders, and how spin correlations come about in this process. Then in section 3 we introduce the phenomenological model, followed by a brief review of the relevant theory for polarized top quark decay, and results on the spin analyzing efficiencies in models where the top quark can decay through a charged Higgs boson. Section 4 describes a Monte Carlo simulation study of these effects, and discusses possible experimental observables. Finally, section 5 contains a summary and the conclusions of this work.

2. Top quark pair production at hadron colliders

We will adopt the latest combined value for the top mass $m_t = 170.9 \pm 1.8\,\text{GeV}$ [47]. Pair production of top quarks occurs in leading order QCD both through $q\bar{q}$ annihilation via an s-channel gluon, and through gluon fusion for which s-, t- and u-channel exchanges are possible. The total hadronic cross section has long been known to NLO accuracy [48, 49]. With CTEQ6 parton distributions [50] and a common choice of scales $\mu_{\text{R}} = \mu_{\text{F}} = m_t$, we obtain $\sigma(pp \rightarrow t\bar{t} + X) \simeq 900$ pb at $\sqrt{s} = 14\,\text{TeV}$ using the NLO MC generator POWHEG [51]. One year of LHC running at low luminosity, corresponding to $\int \mathcal{L} = 10\,\text{fb}^{-1}$, will therefore produce of order 10^7 $t\bar{t}$ events.

Individually unpolarized top quarks are still produced with strong correlations between their spin projections in a suitable basis. The nature and magnitude of these correlations depend on the partonic center of mass (CM) energy. Following [24] we define the production correlation, as a function of the invariant mass $M_{t\bar{t}}$ of the top pair, to be

$$\hat{C}_{ij}(M_{t\bar{t}}^2) = \frac{\hat{\sigma}_{ij}(t_\uparrow \bar{t}_\uparrow + t_\downarrow \bar{t}_\downarrow) - \hat{\sigma}_{ij}(t_\downarrow \bar{t}_\uparrow + t_\uparrow \bar{t}_\downarrow)}{\hat{\sigma}_{ij}(t_\uparrow \bar{t}_\uparrow + t_\downarrow \bar{t}_\downarrow) + \hat{\sigma}_{ij}(t_\downarrow \bar{t}_\uparrow + t_\uparrow \bar{t}_\downarrow)} \tag{2.1}$$

for the partonic subprocess involving initial state partons i, j. Arrows indicate the spin projection on the chosen spin quantization axes (which may be different for t and $\bar{t}$). We choose here to work exclusively in the *helicity basis*, in which the spin is quantized along the momentum directions of the $t(\bar{t})$ in the partonic CM frame. In this basis, the notation (R, L) is sometimes used interchangeably with $(\uparrow, \downarrow)$ to denote the two spin projections.

Near threshold, the $t\bar{t}$ are always produced in an S-wave state. For production dominated by $q\bar{q} \rightarrow t\bar{t}$ through an s-channel gluon, the overall angular momentum state will therefore be $^3S_1$. Out of the three states composing the triplet, two correspond to opposite helicities for the two top quarks, whereas one state gives equal helicities. The combined correlation according to (2.1) is thus $\hat{C}_{q\bar{q}}(4m_t^2) = -1/3$ at threshold. When instead $gg \rightarrow t\bar{t}$ production dominates, which is the case for LHC energies, the situation at threshold is reversed. The top pair is now produced in a singlet $^1S_0$ configuration, since the initial state gluons do not populate $J = 1$ states [20]. In this case the $t\bar{t}$ must always come with the same helicities, which means that $\hat{C}_{gg}(4m_t^2) = 1$. Finally, in the ultra-relativistic limit $(M_{t\bar{t}}^2 \gg 4m_t^2)$, helicity conservation requires the $t\bar{t}$ to have opposite helicities independent of partonic subprocess. Hence the correlation $\hat{C}_{ij}(M_{t\bar{t}}^2) \rightarrow -1$ for all i, j in the high energy limit.

In general, the total statistical correlation $\mathcal{C}$ in a sample of $t\bar{t}$ events is obtained from averaging over the invariant mass of the top pair, while parton distribution functions determine the relative contributions of the competing production processes:

$$\mathcal{C}(s) = \frac{1}{\sigma_{t\bar{t}}} \sum_{i,j = \{q,\bar{q},g\}} \int dx_1 dx_2 \left[\hat{\sigma}_{ij}(t_\uparrow \bar{t}_\uparrow + t_\downarrow \bar{t}_\downarrow) - \hat{\sigma}_{ij}(t_\downarrow \bar{t}_\uparrow + t_\uparrow \bar{t}_\downarrow)\right] f_i(x_1, \mu_{\text{F}}^2) f_j(x_2, \mu_{\text{F}}^2). \tag{2.2}$$

The $\hat{C}_{ij}$ for all partonic subprocesses have previously been calculated to NLO in QCD. From these one obtains $\mathcal{C} = 0.326$ [29] in the helicity basis for pp collisions at $\sqrt{s} = 14\,\text{TeV}$. The residual uncertainty in this number from PDF and scale choices is of order one
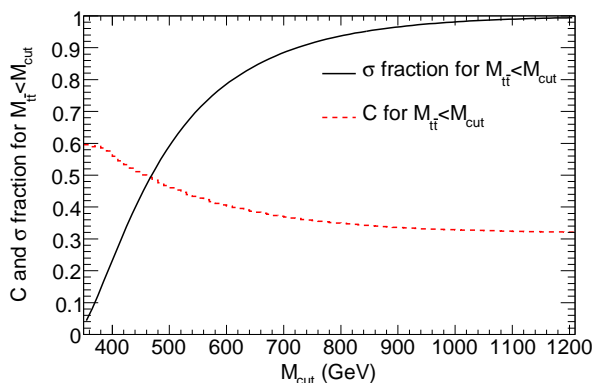
Figure 1: The dashed red curve shows the resulting value of $\mathcal{C}$ in the helicity basis, at the LHC, when a cut $M_{t\bar{t}} < M_{\text{cut}}$ has been applied. The black curve shows the fraction of the total cross section which survives the cut.

percent, a value similar to the difference from the LO calculation which gives $\mathcal{C} = 0.319$. For Tevatron run-II conditions ($p\bar{p}$ collisions at $\sqrt{s} = 1.96\,\text{TeV}$) the same helicity basis correlation becomes $\mathcal{C} = -0.352$. At Tevatron energies, where $q\bar{q}$ annihilation totally dominates $t\bar{t}$ production, there exist also more efficient bases for spin quantization in which correlations as large as $\mathcal{C} = 0.8$ can be obtained [27].

As suggested by the discussion above, it can be beneficial to introduce an experimental cut on $M_{t\bar{t}}$ to increase the spin-purity of the $t\bar{t}$ sample at the cost of decreased efficiency [23]. To increase the component of like-sign helicities in the gluon sample at the LHC requires a cut on the *maximum* $M_{t\bar{t}}$. The effect of such a cut on the correlation parameter $\mathcal{C}$ is shown in figure 1. To illustrate the trade-off between spin-purity and efficiency, figure 1 also presents the fraction of the total cross section which passes a cut on the maximum $M_{t\bar{t}}$. As we have already indicated, $t\bar{t}$ statistics will not be the limiting factor at the LHC. It is therefore good to keep in mind that $\mathcal{C}$ can be increased using this technique, although we do not make explicit use of this fact here.

3. Spin information in top quark decay

In the SM, the top quark decays almost exclusively via the charged current V-A vertex

$$\mathcal{L}_{Wtb} = \frac{g_W}{\sqrt{2}} V_{tb} W^+_\mu \bar{t} \gamma^\mu \frac{1 - \gamma^5}{2} b + \text{h.c.}, \tag{3.1}$$

where $V_{tb} \sim 1$ is the appropriate element of the CKM matrix. In addition to the Standard Model decay, the possibility exists that the top quark decays anomalously. The decay could then contain a small V+A component, or it could be mediated by additional bosons of different spin. The study of spin correlations opens a window on both these possibilities. Our aim here is to explore the latter case, allowing for an extended scalar sector.

Coupling	2HDM (I)	2HDM (II)	2HDM ($\overline{\text{II}}$)
A	$m_u \cot\beta$	$m_u \cot\beta$	$m_u \cot\beta \left[1 - \epsilon'_t \tan\beta\right]$
B	$-m_d \cot\beta$	$m_d \tan\beta$	$\frac{m_d \tan\beta}{1 + \epsilon_b \tan\beta}$
C	$-m_l \cot\beta$	$m_l \tan\beta$	$m_l \tan\beta$

Table 1: CP-invariant couplings of charged Higgs bosons to fermions in 2HDM (I), 2HDM (II) and SUSY-improved type II model ($\overline{\text{II}}$).

3.1 Charged higgs model

Introducing a charged scalar pair $H^\pm$, their interactions with fermions are parametrized by an effective Lagrangian density

$$
\mathcal{L}_H = \frac{g_W}{2\sqrt{2}m_W} \sum_{\substack{\{u,c,t\}\\\{d,s,b\}}} V_{ud} \Bigg\{ H^+ \bar{u}\Big[A\left(1-\gamma_5\right)+B\left(1+\gamma_5\right)\Big]d + H^- \bar{d}\Big[B^*\left(1-\gamma_5\right)+A^*\left(1+\gamma_5\right)\Big]u\Bigg\}
$$
$$
+ \frac{g_W}{2\sqrt{2}m_W} \sum_{\{e,\mu,\tau\}} \Big[H^+ C\bar{\nu}_l\left(1+\gamma_5\right)l + H^- C^*\bar{l}\left(1-\gamma_5\right)\nu_l\Big]. \tag{3.2}
$$

The A, B, C, and their complex conjugates, are in principle free parameters determining the Lorentz structure of the couplings. Note that this model does not assign definite parity to the $H^\pm$ unless $B = \pm A$. For $AB = 0$ parity is violated maximally. Assuming CP-invariance of the scalar sector, the coupling parameters can all be taken as real numbers.

A model such as (3.2) occurs, for example, as the charged Higgs-fermion sector of a two Higgs Doublet Model (2HDM). Here, the SM Higgs sector is augmented with another complex Higgs doublet, resulting in two charge conjugate ($H^\pm$) and three neutral (h, H, A) states occurring as physical bosons. To ensure the augmented SM does not allow for tree-level FCNC's, certain restrictions apply on how to couple the extended Higgs sector to the fermions. For our purposes, it suffices to say that two options are generally considered: In the so-called type I model [2HDM (I)], only one doublet is coupled directly to the fermions. In the type II model [2HDM (II)], one doublet is coupled only to up-type fermions, whereas the other doublet couples only to down-type fermions.

The number of independent parameters in the Higgs sector is thereby restricted to two at leading order. We will adopt for these the ratio $\tan\beta = v_2/v_1$ of the two doublets vacuum expectation values, and the charged Higgs mass m_{H^+}. For the two model types, the charged Higgs-fermion couplings are then given in table 1. Mass parameters appearing in the couplings should be evaluated at a scale $Q^2 = m_{H^+}^2$, using the $\overline{\text{MS}}$ masses $\overline{m}_q(Q^2)$ to ensure proper resummation of large logarithmic QCD vertex corrections [52–54]. Since the $H^\pm$ couples proportionally to the fermion mass, we will only be concerned with third generation particles in the following.

As discussed in the introduction, one possible extension of the Standard Model where a 2HDM occurs naturally is the Minimal Supersymmetric Standard Model (MSSM). The

MSSM contains a 2HDM (II), but since the supersymmetry introduces additional particles, the two-parameter picture of the 2HDM (II) works only as an effective tree-level description. It has been shown [52, 55], that quantum corrections due to SUSY-QCD loops can be quite sizable for large values of $\tan\beta$. This holds even in the decoupling limit when all SUSY masses are taken to infinity. How these corrections enter into the effective $H^\pm$ couplings can be seen from the third column of table 1. We will call the 2HDM which includes the $\tan\beta$ enhanced SUSY corrections the "modified type II", or simply $\overline{\text{II}}$. The corrections are of two types: first the so-called ϵ_b correction to the relation between the bottom quark mass m_b and the bottom Yukawa coupling y_b. It is caused by gluino-sbottom and chargino-stop loops. At one-loop, the dominant contributions to this correction are given by [56, 55]

$$\epsilon_b = -\frac{2\alpha_s}{3\pi}\frac{\mu}{m_{\tilde{g}}}H_2\left(\frac{m_{\tilde{b}_1}}{m_{\tilde{g}}},\frac{m_{\tilde{b}_2}}{m_{\tilde{g}}}\right) - \frac{y_t^2}{16\pi^2}\tilde{U}_{a2}\frac{A_t}{m_{\tilde{\chi}_a^+}}H_2\left(\frac{m_{\tilde{t}_1}}{m_{\tilde{\chi}_a^+}},\frac{m_{\tilde{t}_2}}{m_{\tilde{\chi}_a^+}}\right)\tilde{V}_{a2}, \qquad (3.3)$$

which introduces a dependence on the trilinear coupling A_t, the top Yukawa coupling y_t, and the μ parameter from the superpotential — in addition to the dependence on several of the sparticle masses. The real matrices $\tilde{U}$ and $\tilde{V}$ diagonalize the chargino mass matrix. The function H_2 is given by

$$H_2(x,y) = \frac{x\ln x}{(1-x)(x-y)} + \frac{y\ln y}{(1-y)(y-x)}. \qquad (3.4)$$

In the limit when all SUSY parameters and sparticle masses are of similar scale M_{SUSY} one obtains $|\epsilon_b| \simeq \alpha_s(Q = M_{\text{SUSY}})/(3\pi) \sim 10^{-2}$. The sign of ϵ_b is determined by the sign of μ.

The second contribution which modifies the $H^\pm$ couplings is [55]

$$\begin{aligned}
\epsilon_t' = &-\frac{2\alpha_s}{3\pi}\frac{\mu}{m_{\tilde{g}}}\left[c_{\tilde{t}}^2c_{\tilde{b}}^2 H_2\left(\frac{m_{\tilde{t}_2}}{m_{\tilde{g}}},\frac{m_{\tilde{b}_1}}{m_{\tilde{g}}}\right) + c_{\tilde{t}}^2s_{\tilde{b}}^2 H_2\left(\frac{m_{\tilde{t}_2}}{m_{\tilde{g}}},\frac{m_{\tilde{b}_2}}{m_{\tilde{g}}}\right)\right. \\
&\left. + s_{\tilde{t}}^2c_{\tilde{b}}^2 H_2\left(\frac{m_{\tilde{t}_1}}{m_{\tilde{g}}},\frac{m_{\tilde{b}_1}}{m_{\tilde{g}}}\right) + s_{\tilde{t}}^2s_{\tilde{b}}^2 H_2\left(\frac{m_{\tilde{t}_1}}{m_{\tilde{g}}},\frac{m_{\tilde{b}_2}}{m_{\tilde{g}}}\right)\right] - \\
&-\frac{y_b^2}{16\pi^2}N_{4a}^*\frac{A_b}{m_{\tilde{\chi}_a^0}}\left[c_{\tilde{t}}^2c_{\tilde{b}}^2 H_2\left(\frac{m_{\tilde{t}_1}}{m_{\tilde{\chi}_a^0}},\frac{m_{\tilde{b}_2}}{m_{\tilde{\chi}_a^0}}\right) + c_{\tilde{t}}^2s_{\tilde{b}}^2 H_2\left(\frac{m_{\tilde{t}_1}}{m_{\tilde{\chi}_a^0}},\frac{m_{\tilde{b}_1}}{m_{\tilde{\chi}_a^0}}\right)\right. \\
&\left. + s_{\tilde{t}}^2c_{\tilde{b}}^2 H_2\left(\frac{m_{\tilde{t}_2}}{m_{\tilde{\chi}_a^0}},\frac{m_{\tilde{b}_2}}{m_{\tilde{\chi}_a^0}}\right) + s_{\tilde{t}}^2s_{\tilde{b}}^2 H_2\left(\frac{m_{\tilde{t}_2}}{m_{\tilde{\chi}_a^0}},\frac{m_{\tilde{b}_1}}{m_{\tilde{\chi}_a^0}}\right)\right] N_{a3},
\end{aligned} \qquad (3.5)$$

where the matrix N diagonalizes the neutralino mass matrix, $s_{\tilde{q}} = \sin\theta_{\tilde{q}}$ and $c_{\tilde{q}} = \cos\theta_{\tilde{q}}$ for the squark mixing angles $\theta_{\tilde{q}}$. The squark mass eigenstates are given by $\tilde{q}_1 = c_{\tilde{q}}\tilde{q}_{\text{L}} + s_{\tilde{q}}\tilde{q}_{\text{R}}$ and $\tilde{q}_2 = -s_{\tilde{q}}\tilde{q}_{\text{L}} + c_{\tilde{q}}\tilde{q}_{\text{R}}$, with $m_{\tilde{q}_1} > m_{\tilde{q}_2}$. We note that ϵ_t' is numerically similar to ϵ_b in the case with a common scale for the SUSY parameters. In section 3.5, we will return to these SUSY corrections when discussing numerical results for the 2HDM. As we will show, it turns out that their effects on $t\bar{t}$ spin correlation observables are small.
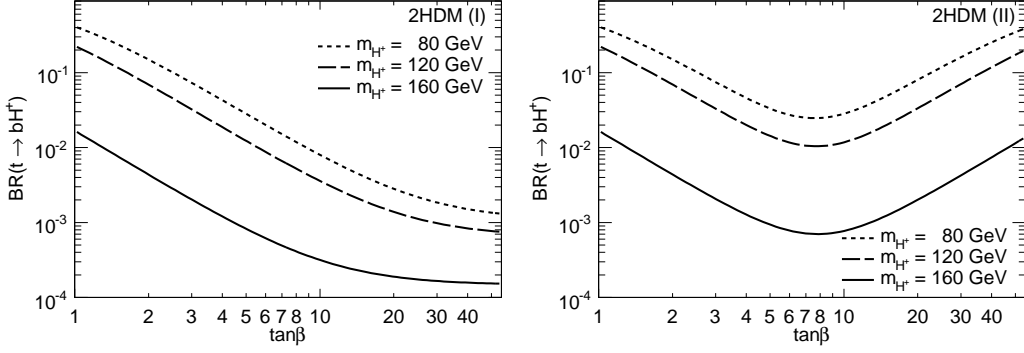
Figure 2: Branching fractions for $t \to bH^+$ in 2HDM (I) (left) and 2HDM (II) (right), as a function of $\tan\beta$. The contours show $m_{H^+} = 80\,\text{GeV}$ (short-dashed), $m_{H^+} = 120\,\text{GeV}$ (long-dashed), and $m_{H^+} = 160\,\text{GeV}$ (solid).

3.2 Top quark decay with polarization

Assuming that the full width Γ_t of the top quark, including the scalar decay mode, is still very small ($\Gamma_t/m_t \lesssim 0.01$) we use the narrow width approximation to factorize the production from the decay of the heavy quarks. The branching fractions for $t \to bH^+$ are shown in figure 2 for 2HDM type (I) and (II). It is clear that type (II) is interesting both for small and large $\tan\beta$ values, whereas the 2HDM (I) only allows a significant $\mathcal{BR}(t \to bH^+)$ for small $\tan\beta$. In the following we will mostly be concerned with the type (II) model.

We treat the decaying $t\bar{t}$ as independent decays through well-defined channels without interference effects. Strictly speaking, a more complete formalism involving off-diagonal $W^\pm/H^\pm$ propagator elements could be used when $m_{H^+} \simeq m_W$. Ignoring such complications, the full structure of density matrices in the $2 \to 6$ matrix element becomes

$$|\mathcal{M}(2 \to 6)|^2 = [R_{\lambda\lambda'\kappa\kappa'}(2 \to t\bar{t}) \otimes \rho^i_{\lambda\lambda'}(t \to 3) \otimes \rho^j_{\kappa\kappa'}(\bar{t} \to 3)]. \tag{3.6}$$

R is here the fully helicity-dependent spin density matrix for $t\bar{t}$ production. The $\rho(\bar{\rho})$ are decay density matrices of $t(\bar{t})$, where i, j label the available decay channels and λ, λ' (κ, κ') are helicity indices for the $t(\bar{t})$.

To obtain the decay density matrix for a given channel, we use the techniques described in appendix A. With momenta defined in figure 3, the leading order decay density matrix elements for semi-leptonic weak decay of the top quark are given by

$$\rho^W_{\lambda\lambda'} = |\mathcal{M}_{\lambda\lambda'}(t \to bW^+ \to bl^+\nu_l)|^2 = \frac{2g_W^4|V_{tb}|^2(p \cdot k_2)(k_1 \cdot k_3)}{(q^2 - m_W^2)^2 + m_W^2\Gamma_W^2}\left[\delta_{\lambda\lambda'} + \hat{k}_2^a\sigma^a_{\lambda\lambda'}\right] \tag{3.7}$$

when the spins of all outgoing particles are summed over. The unit 3-vector $\hat{k}_2$ is given in the rest frame of the decaying quark. For hadronic decay of the W boson, the matrix elements are exactly the same if a) all final state masses are neglected and b) the leptons are replaced by their quark counterparts in terms of weak isospin. CP-invariance of the decay ensures that $|\mathcal{M}_{\lambda\lambda'}(t \to bl^+\nu_l)|^2 = |\mathcal{M}_{\lambda'\lambda}(\bar{t} \to \bar{b}l^-\bar{\nu}_l)|^2$.
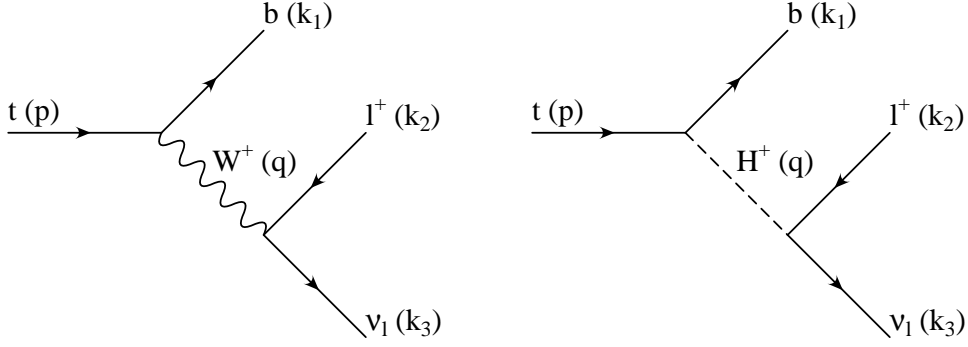
Figure 3: Notation for momenta in semi-leptonic top quark decay mediated either by W^+ or H^+. In hadronic decay of the boson, we use the same notation while making the replacements of weak isospin partners: $l^+ \to \bar{d}$, and $\nu_l \to u$.

Reckon similarly the elements of the decay density matrix when the decay is mediated by a charged scalar as defined by the model (3.2). In this case, the elements become

$$\rho_{\lambda\lambda'}^H = |\mathcal{M}_{\lambda\lambda'}(t \to bH^+ \to bl^+\nu_l)|^2 = \frac{g_W^4 |V_{tb}|^2 (p \cdot k_1)(k_2 \cdot k_3)}{(q^2 - m_{H^+}^2)^2 + m_{H^+}^2 \Gamma_{H^+}^2} \frac{C^2(A^2 + B^2)}{2m_W^4} \quad (3.8)$$

$$\times \left(1 + \frac{AB}{A^2 + B^2} \frac{4\delta}{1 - \xi}\right) \left[\delta_{\lambda\lambda'} - \frac{A^2 - B^2}{A^2 + B^2} \left(1 + \frac{AB}{A^2 + B^2} \frac{4\delta}{1 - \xi}\right)^{-1} \hat{k}_1^a \sigma_{\lambda\lambda'}^a\right].$$

Here the notation $\xi = m_{H^+}^2/m_t^2$ and $\delta = m_b/m_t$ is used. Let us also introduce a convenient short-hand

$$f(\xi, A, B) = \left(1 + \frac{AB}{A^2 + B^2} \frac{4\delta}{1 - \xi}\right)^{-1} \quad (3.9)$$

for the threshold factor. This function has the general properties $f(\xi, A, B) = 1$ for $m_{H^+} \ll m_t$, and $f(\xi, A, B) \to 0$ for $\xi \to 1$, unless $AB = 0$.

3.3 W boson helicity

The perhaps most direct test of V-A theory in top quark decay is offered by examining the polarization states of the W boson mediating the decay. Due to the large Yukawa coupling $y_t \sim 1$, a fraction $m_t^2/(m_t^2 + 2m_W^2) \simeq 0.69$ of the W bosons are expected to be longitudinally polarized, while the remainder carries a left-handed helicity in the t rest frame. Uncertainties in these numbers from higher order corrections, including virtual 2HDM and SUSY effects, are under control at the 1% level [57, 58].

When the W decays further, the angular dependencies of the decay products on the different helicity states are given by the Wigner d-functions for the spin 1 representation. Combining this knowledge with the matrix element for $t \to bW^+$, the normalized lepton angular distribution in leptonic decay of the W is given by

$$\frac{1}{N} \frac{\mathrm{d}N(W \to l\nu_l)}{\mathrm{d}\cos\theta_l^*} = \frac{3}{4(m_t^2 + 2M_W^2)} \left[m_t^2 \sin^2\theta_l^* + M_W^2 (1 - \cos\theta_l^*)^2\right], \quad (3.10)$$

where θ_l^* is defined in the W rest system as the angle of the lepton momentum to the W helicity axis. Using the fact that, in the rest frame of the decaying top, the recoiling b quark has its momentum anti-parallel to that of the W, the lepton helicity angle $\cos \theta_l^*$ can be determined by the invariant product [59]

$$\cos \theta_l^* = \frac{k_1 \cdot (k_2 - k_3)}{k_1 \cdot (k_2 + k_3)} \qquad (3.11)$$

if the b mass is neglected. Assuming further that the decay is mediated through an on-shell W, the approximate expression

$$\cos \theta_l^* \simeq \frac{4 k_1 \cdot k_2}{m_t^2 - m_W^2} - 1 \qquad (3.12)$$

can be obtained from the kinematics of the decay. The form (3.12) is experimentally advantageous since no knowledge of the neutrino momenta is required to determine $\cos \theta_l^*$. Being only an approximate on-shell relation, the values obtained using this expression may in reality be such that $|\cos \theta_l^*| > 1$ for some events.

In the decay of a charged Higgs boson, the decay products should be isotropically distributed in $\cos \theta^*$. This offers a clear signature for a new charged boson to have spin 0. However, even with a large branching ratio $t \to bH^+$, this appreciable difference would not contribute much to measurements of the distribution (3.10) using electrons or muons, simply because in the $\tan \beta$ regions of interest, $\mathcal{BR}(H^\pm \to \tau^\pm \nu_\tau) \simeq 1$ in the 2HDM.[1] If, at the LHC, evidence starts to gather in favor of a light $H^\pm$, it would therefore be interesting to study the angular distribution of τ leptons exclusively using the hadronic τ decay. Experimentally this presents a formidable task, since the presence of two final state neutrinos in the τ channel introduces ambiguities in the reconstruction of the τ momentum. Furthermore, when $m_{H^+} > m_W$, the kinematic assumptions behind Equation (3.12) are no longer valid. It is then natural to exploit these kinematic differences fully and treat the two decays separately also in the angular analysis in order to establish the spin 0 nature of the presumptive $H^\pm$.

In figure 4, we show the angular distribution of τ leptons in the rest system of the boson mediating the $t(\bar{t})$ decay. We show here the expectations for the SM, given by Equation 3.10, and mixtures of SM+2HDM (II) with $\mathcal{BR}(t \to bH^+)$ corresponding to three different values of $\tan \beta$. It is assumed either that $m_{H^+} = 80 \,\mathrm{GeV}$, or that kinematic effects can be compensated for on event-by-event basis. Even for $\mathcal{BR}(t \to bH^+) \lesssim 0.1$, the $H^\pm$ events give a significant contribution since $\mathcal{BR}(W^\pm \to \tau^\pm \nu_\tau) = 0.1125 \pm 0.0020$ is equally small.

3.4 Polarization observables

From the matrix elements (3.7) and (3.8) some useful hints are obtained on how the spin is analyzed in top quark decays. The spin-dependent term, proportional to $\sigma_{\lambda \lambda'}$, appears

---

[1]A small contamination from $H^\pm \to \tau^\pm \nu_\tau \to l^\pm \nu_l \nu_\tau \bar{\nu}_\tau$ would of course be present also in the lepton samples in these cases.
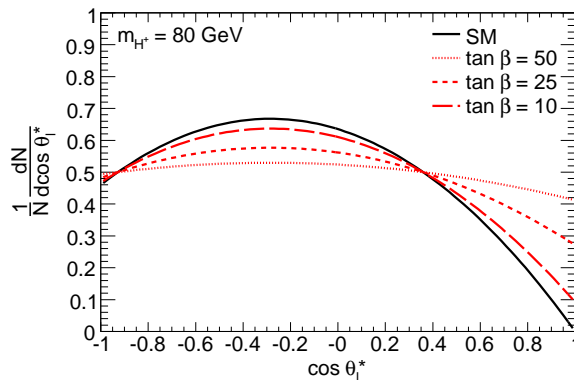
Figure 4: Angular distribution of τ leptons in the rest system of the boson mediating top quark decay. The curves show the SM (black solid), and SM+2HDM (II) with $m_{H^+} = 80\,\text{GeV}$ for three different values of $\tan\beta$: 50 (dotted), 25 (short-dashed), and 10 (long-dashed). $\mathcal{BR}(H^+ \to \tau^+\nu_\tau) = 1$ was assumed for all values of $\tan\beta$. In the low $\tan\beta$ regime, the same distributions are obtained whenever $\mathcal{BR}(t \to bH^+) \times \mathcal{BR}(H^+ \to \tau^+\nu_\tau)$ is the same.

with different associated momentum directions in the two channels. The particle with this momentum will analyze the spin most effectively in the corresponding case. To see how this comes about, recall [60] how the spin of a given top quark is analyzed. The decay products will experience angular distributions reflecting the spin state of the parent. Each polarized partial width $\Gamma(t_\uparrow \to bX^+ \to bl^+\nu_l)$ of a decaying fermion can be put in the form

$$\frac{1}{\Gamma}\frac{\mathrm{d}\Gamma}{\mathrm{d}\cos\theta_i} = \frac{1 + \alpha_i \cos\theta_i}{2}, \tag{3.13}$$

where θ_i denotes the angle of decay product i to the spin helicity axis, calculated in the rest frame of the decaying particle. The *spin analyzing coefficients* α_i determine the efficiency of a given particle to analyze the spin of the parent. The factorization of Γ in energy-dependent and angular parts holds to a high degree also when including radiative QCD corrections [60].

To obtain the full set of α_i for a given decay, it is necessary to integrate the polarized matrix elements. Using the kinematic variables $x = 2p \cdot k_2/m_t^2$ and $y = (k_2 + k_3)^2/m_t^2$, the Dalitz parametrization [61] of the 3-body phase space is written as

$$\mathrm{d}\Phi_3 = \frac{1}{(2\pi)^5}\mathrm{d}x\mathrm{d}y\mathrm{d}\gamma\mathrm{d}\beta\mathrm{d}\cos\theta. \tag{3.14}$$

The three Euler angles γ, β, and θ are here chosen according to [62], so that θ coincides with the helicity angle θ_i discussed above. The integration over β is always trivial and gives 2π. The integration over γ is non-trivial only for two, spin-dependent, quantities. With positive spin projection along the helicity axis, the result is

$$\int \mathrm{d}\gamma\; s \cdot k_1 = 2\pi\cos\theta\left[\frac{1}{2}\left(1 + y - \delta^2\right) - \frac{y}{x}\right]m_t^2$$

Analyzing	Decay channel	
particle	W^+ $(\omega = m_W^2/m_t^2)$	H^+ $(\xi = m_{H^+}^2/m_t^2)$
b	$-\dfrac{1-2\omega}{1+2\omega}$	$-\dfrac{A^2-B^2}{A^2+B^2}f(\xi,A,B)$
W^+/H^+	$\dfrac{1-2\omega}{1+2\omega}$	$\dfrac{A^2-B^2}{A^2+B^2}f(\xi,A,B)$
l^+ $(\bar d)$	1	$\dfrac{1-\xi^2+2\xi\ln\xi}{(1-\xi)^2}\dfrac{A^2-B^2}{A^2+B^2}f(\xi,A,B)$
ν_l (u)	$\dfrac{(1-\omega)(1-11\omega-2\omega^2)-12\omega^2\ln\omega}{(1-\omega)^2(1+2\omega)}$	$-\dfrac{1-\xi^2+2\xi\ln\xi}{(1-\xi)^2}\dfrac{A^2-B^2}{A^2+B^2}f(\xi,A,B)$

Table 2: Spin analyzing coefficients α_i for different decay products in SM and scalar decay of a polarized top quark $(t_\uparrow \to bW^+/H^+ \to bl^+\nu_l)$, or equivalently $(t_\uparrow \to bW^+/H^+ \to b\bar d u)$.

and since $\sum_i k_i \cdot s = p \cdot s = 0$, with $k_2 \cdot s = -\cos\theta\frac{x}{2}m_t^2$, the other interesting integral becomes

$$\int \mathrm{d}\gamma\ s \cdot k_3 = 2\pi\cos\theta\left[\frac{y}{x}-\frac{1}{2}(1+y-x-\delta^2)\right]m_t^2.$$

The coefficients α_i have been determined for both decay channels. We summarize our results in table 2 for a decaying t with positive helicity. Expressions for the other helicity state, or for the charge conjugate $\bar t$ decay, are obtained by an overall change of sign. Our results agree with those presented in [23], except that their expressions for the scalar case do not contain the factor $(A^2-B^2)/(A^2+B^2)f(\xi,A,B)$. This factor contains all the dependence of the spin analyzing power on the Lorentz structure of the coupling. We note further that the expression we obtain for α_H is in agreement with that of [44], where also $\mathcal{O}(\alpha_s)$ corrections to this quantity are given. The inclusion of NLO corrections does not modify the $\tan\beta$ dependence of the α_i, even if the numerical values are slightly altered. Since we aim to compare the analytic results to a LO Monte Carlo simulation, we use only the LO results for α_i throughout this work.

Since the top quark spins are not directly observable themselves, what will be accessible are quantities constructed only from final state momenta. The most direct such being the doubly differential distributions of the same type as in Equation (3.13), but now involving two particles (i,j); one from each decaying top quark. The helicity angles θ_i and θ_j are then calculated in the rest systems of the respective parents.[2] The most general expression of this type is

$$\frac{1}{N}\frac{\mathrm{d}^2N}{\mathrm{d}\cos\theta_i\mathrm{d}\cos\theta_j} = \frac{1}{4}\Big(1+P_1\alpha_i\cos\theta_i+P_2\alpha_j\cos\theta_j+\mathcal{C}\alpha_i\alpha_j\cos\theta_i\cos\theta_j\Big) \qquad (3.15)$$

where $P_1(P_2)$ measures the degrees of transverse polarization of the $t(\bar t)$. $\mathcal{C}$ is the correlation parameter discussed in section 2. In leading order QCD, with the spin quantized in the

---

[2]We use the convention of performing rotation-free boosts from the $t\bar t$ CM system to define the orientation of the $t(\bar t)$ rest systems. Alternatively, one could perform a rotation-free boost directly from the hadronic CM system.

helicity basis, $P_1 = P_2 = 0$ by parity invariance. Instead of (3.15) the simpler distribution

$$\frac{1}{N} \frac{\mathrm{d}^2 N}{\mathrm{d}\cos\theta_i \, \mathrm{d}\cos\theta_j} = \frac{1}{4}\Big(1 + \mathcal{C}\alpha_i\alpha_j \cos\theta_i \cos\theta_j\Big) \tag{3.16}$$

is therefore expected to obtain.

It is also possible to form one-dimensional distributions, e.g. as studied in [29]. If we define the angle θ_{ij} between the vectors i and j as in the previous distribution, we get

$$\frac{1}{N} \frac{\mathrm{d}N}{\mathrm{d}\cos\theta_{ij}} = \frac{1}{2} \left(1 + \mathcal{D}\alpha_i\alpha_j \cos\theta_{ij}\right). \tag{3.17}$$

Here the coefficient $\mathcal{D}$ is related to $\mathcal{C}$, but in general it has a different value. With a leading order $\mathcal{C} = 0.319$, we obtain the corresponding $\mathcal{D} = -0.216$. To determine $\mathcal{C}$ and $\mathcal{D}$ from angular distributions, the relations

$$\mathcal{C} = \frac{9}{\alpha_i\alpha_j} \langle \cos\theta_i \cos\theta_j \rangle \tag{3.18}$$

$$\mathcal{D} = \frac{3}{\alpha_i\alpha_j} \langle \cos\theta_{ij} \rangle \tag{3.19}$$

can be used. Conversely, when the correlation coefficients are known, these relations can be used to determine the product $\alpha_i\alpha_j$.

3.5 Analysis in 2HDM (II)

As an illustrative example of the differences between the SM and a new scalar decay, let us consider in some detail the results for a 2HDM (II) with $H^\pm$ couplings from table 1. In all the following, we shall fix the top mass to $m_t = 170.9\,\mathrm{GeV}$ [47]. Starting by analyzing the threshold region $m_{H^+} \simeq m_t - m_b$, figure 5 shows α_H as a function of m_{H^+} for different values of $\tan\beta$. We see that the threshold suppression becomes significant as m_{H^+} approaches the kinematic limit. However, for very large, very small or intermediate (~ 7) $\tan\beta$ values, we infer the threshold correction to be less than 10% also for $m_{H^+} = 160\,\mathrm{GeV}$. In these regions of parameter space, the threshold factor can be effectively ignored. Note that this argument is not specific to α_H, but applies to all α_i, since $f(\xi, A, B)$ is a universal factor.

Summarizing the results presented in table 2 for the 2HDM (II), figure 6 shows a numerical evaluation of the analytic expressions for all α_i. The results are presented for two values of $\tan\beta$: one large value ($\tan\beta = 50$), for which the efficiency in analyzing the spin is optimum, and one intermediate value $\tan\beta = \sqrt{m_t/\overline{m}_b} \sim 8$ (for $\overline{m}_b = 3.2\,\mathrm{GeV}$ with $m_{H^+} = 100\,\mathrm{GeV}$), where all the sensitivity to analyze the top spin vanishes. This value corresponds to a purely scalar coupling, thus to an isotropic decay. For $\tan\beta \lesssim 8$, all α_i acquire an extra minus sign compared to $\tan\beta \gtrsim 8$. This corresponds to a shift from predominantly right-chiral to left-chiral coupling. We see also, that the efficiency to analyze the top spin is not highest using the charged lepton, as is shown to be the case for the SM. Instead the most efficient probe is either the Higgs momentum itself or the associated b quark. This is easily understood; since the $H^\pm$ itself does not carry any spin, the top spin information can only be transferred to the angular distributions of the b/H^+.
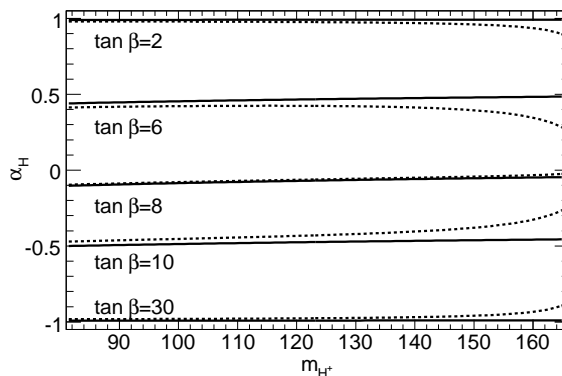
Figure 5: Influence of the threshold factor on the spin analyzing coefficients. The dashed curves show the full expression for α_H while the solid curves show α_H in the approximation $f(\xi, A, B) = 1$
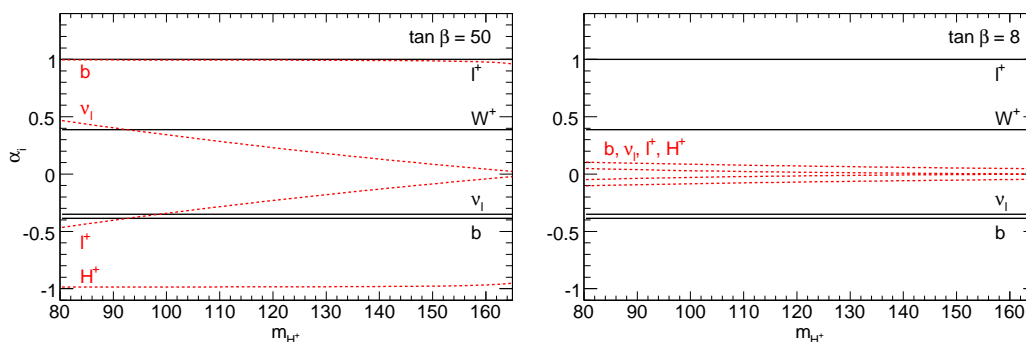

Figure 6: Spin analyzing coefficients α_i for top decay within SM (solid black), and in the 2HDM (II) (dashed red), presented for $\tan\beta = 50$ (left) and $\tan\beta = 8$ (right). For low $\tan\beta \sim 1$, the Higgs results presented in the left plot are valid with an overall change of sign.

In a vector decay, parts of this information go into the different polarization states of the W, as discussed above.

Figure 7 displays α_b as a function of $\tan\beta$ for a fixed $m_{H^+} = 100\,\text{GeV}$. It illustrates clearly the transition from $\alpha_b = -1$ analyzing power at small $\tan\beta$, to $\alpha_b = 1$ associated with a right handed coupling for large $\tan\beta$. Note also, that for $\tan\beta = \sqrt{\sqrt{2}\frac{m_W}{\overline{m}_b}} \sim 6$, the b quark coefficient α_b of the Higgs events mimics that of the SM decay. The only dependence in this relation on m_{H^+} enters through the running mass $\overline{m}_b$. No corresponding $\tan\beta$ value exists where the α_l are equal, since the Higgs value is bounded by kinematics to $|\alpha_l| \lesssim 0.5$, whereas the SM value is always $\alpha_l = 1$.

To compare with the case when $\tan\beta$-enhanced SUSY corrections to the charged Higgs couplings are included, we give in figure 7 also the values of α_b for the 2HDM ($\overline{\text{II}}$). Rather than to calculate the corrections for a specific SUSY model spectrum, we parametrize them in terms of the parameters $|\epsilon_b| \leq 0.01$ and $|\epsilon'_t| \leq 0.01$. These are reasonable maximum values [55], which correspond roughly to $\alpha_s/3\pi$ as discussed above. Figure 7 clearly shows
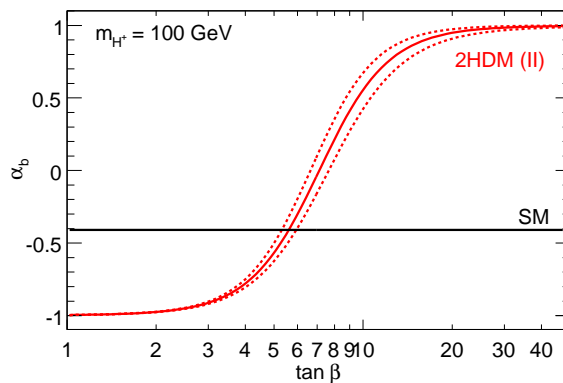
Figure 7: The solid red curve shows α_b for the 2HDM (II), whereas the dashed curves correspond to the SUSY-corrected model $(\overline{\text{II}})$ with $\epsilon_b = -\epsilon'_t = \pm 0.01$. The mass $m_{H^+} = 100\,\text{GeV}$ was used. For comparison, the black line shows α_b for the SM decay.

that even though these corrections are enhanced by $\tan\beta$ in the couplings, they have only a small effect on the ratio that enters the spin analyzing coefficients. In fact, the largest correction is obtained not in the high $\tan\beta$ limit, but in the transition region around $\tan\beta = 8 - 20$. Given the observed smallness of the SUSY effects on the spin analyzing coefficients, it is acceptable to apply the results from the 2HDM (II) without modification, both in the high and in the low $\tan\beta$ regimes. However, total rates for $t \to bH^+$ are of course affected by the differences.

A few words are to be said also about the $\mathcal{O}(\alpha_s)$ corrections calculated in [44]. Inclusion of these effects leads to modifications of the spin analyzing coefficients in a fashion very similar to the $\tan\beta$ enhanced SUSY corrections discussed above. These corrections are also largest in the intermediate $\tan\beta$ region, where they can reach 20% in magnitude. In the large and small $\tan\beta$ limits, the NLO corrections have negligible impact. Since our results are most interesting in these limits, we will show plots for $\tan\beta = 50$ and $\tan\beta = 1$. Interpolation to the intermediate range should then be performed with care, remembering the higher order corrections.

As a final result for the 2HDM (II) on matrix element level, we show the differential distributions in $(\cos\theta_i, \cos\theta_j)$ and $\cos\theta_{ij}$, described by equations (3.16) and (3.17) respectively. The top row in figure 8 shows "lepton-lepton" correlations, where the lepton (d quark) from a W decay is correlated with another lepton (in this case a τ) from $W^\pm$ or $H^\pm$ decay from the opposite side of the event. In the absence of $t\bar{t}$ spin correlations, this distribution is expected to be flat. From left to right, figure 8 gives the results for the SM, for the 2HDM (II) with $\tan\beta = 50$, and similarly with $\tan\beta = 1$. In the bottom row, distributions in one of the angles are given. These are obtained using the other angle to determine the parent top quark spin by applying the projections $\cos\theta_d > 0$ and $\cos\theta_d < 0$ to the 2D distributions. Figure 8 illustrates the points we have previously made about the 2HDM (II), namely that i) the lepton-lepton correlation is more efficient in the SM since $\alpha_l \neq 1$ in the Higgs case, ii) there is a change of sign in going from high to low values of
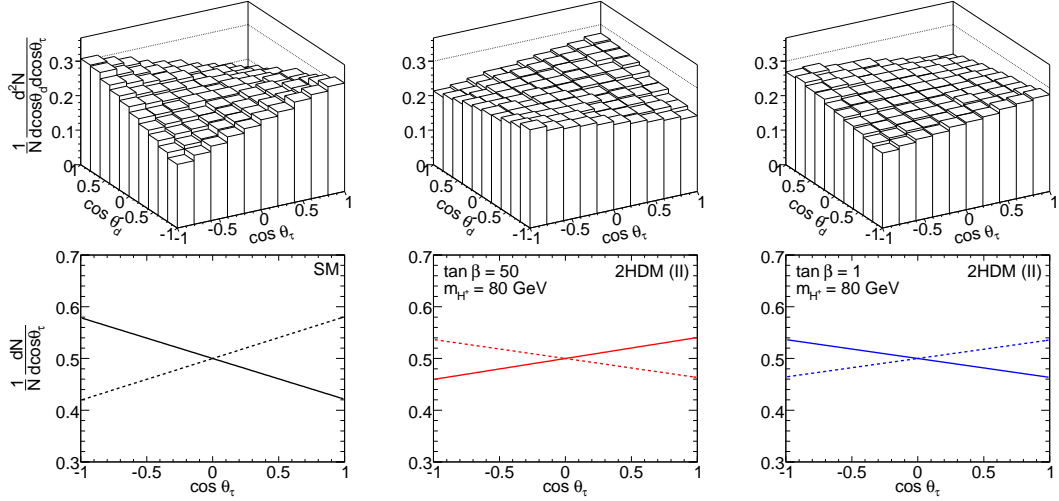
Figure 8: Upper row shows doubly differential distributions in $\cos\theta_{i,j}$ (defined in the text) of the decay products d and τ from $t\bar{t}$ decaying through $W^{\pm}W^{\mp}$ (left) and $H^{\pm}W^{\mp}$ (center, right). Results obtained at ME level for $m_{H^+} = 80\,\mathrm{GeV}$, $\tan\beta = 50$ (center) and $\tan\beta = 1$ (right). The bottom panel lines correspond to projected angular distributions with $\cos\theta_d > 0$ (solid) and $\cos\theta_d < 0$ (dashed).
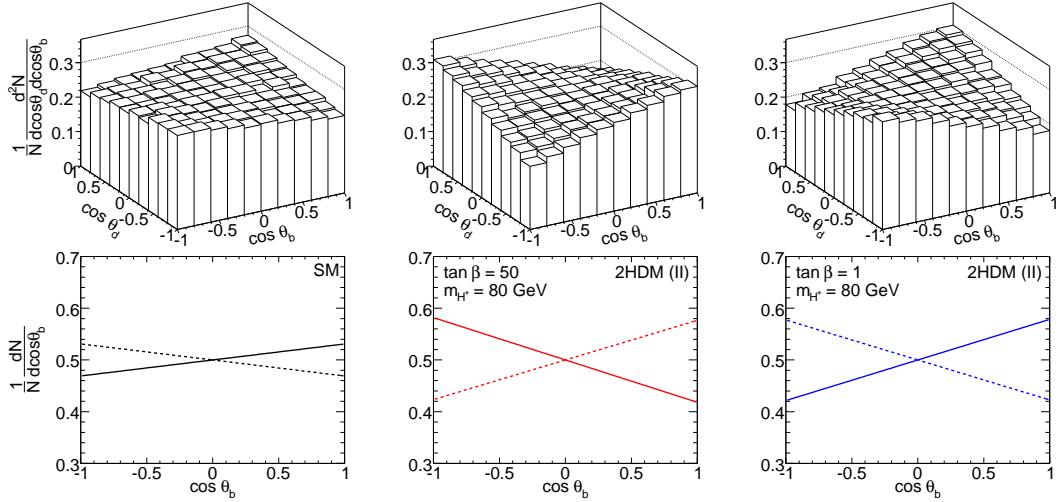

Figure 9: Angular distributions defined similarly to those in figure 8, with the τ replaced by the associated b quark originating from the same $t(\bar{t})$ decay. Again $m_{H^+} = 80\,\mathrm{GeV}$ and the ordering is SM (left), $\tan\beta = 50$ (center), and $\tan\beta = 1$ (right).

$\tan\beta$, and iii) the low $\tan\beta$ case is more SM-like.

Going to figure 9, the τ lepton has been replaced with the b quark associated with the same (Higgs) side of the event. The three distributions are defined similarly to those in figure 8, as are the projections. From figure 9, the increased spin analyzing efficiency when using the associated b quark in the Higgs case is evident.
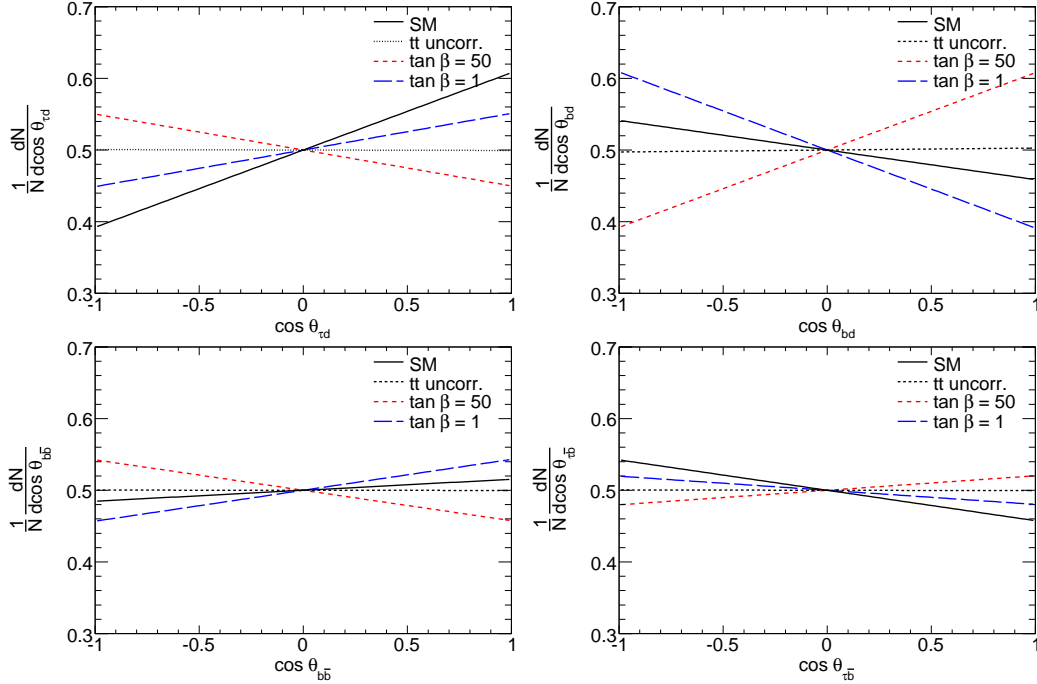
Figure 10: Distributions at matrix element level of $\cos\theta_{ij}$ for different final state particles (i, j). The dotted line is the expected SM result *without $t\bar{t}$* spin correlations. The SM result is shown in black, while the 2HDM (II) is presented for $\tan\beta = 1$ (long-dashed blue), and $\tan\beta = 50$ (short-dashed red). All results are given for $m_{H^+} = 80\,\text{GeV}$.

The last figure to discuss here is figure 10, which shows distributions in $\cos\theta_{ij}$ between different particles in the final state. An uncorrelated sample corresponds to a flat line distribution. The specific combinations chosen are (τ, d), (b, d), $(b, \bar{b})$, and $(\tau, \bar{b})$, where the first particle originates from $H^\pm/W^\pm$ decay, while the second always comes from the opposite side $W^\pm$. The distributions $(H^+, \bar{b})$ and (H^+, d) are equivalent to the distributions $(b, \bar{b})$ and (b, d) displayed in figure 10 with a change of sign in the spin analyzing coefficient $(\alpha_H = -\alpha_b$ in eq. (3.17)). Hence they do not contain any additional information.

By combining in the same plots results for the SM with results from the 2HDM, we see directly which correlations are more efficient in the two cases. In agreement with previous results, this is again the (τ, d) distribution for the SM, and the $(b, \bar{b})$ distribution for the 2HDM (II), illustrating the universal dependence of the spin correlation effects on $\alpha_i\alpha_j$. We have also found, that when phase-space cuts are applied at the parton level, the distributions shown in figure 10 are not affected nearly as much as those presented in figures 8 and 9. Using the $\cos\theta_{ij}$ variables to study $t\bar{t}$ spin correlations is therefore advantageous to avoid the problems with cuts discussed in [23]. We will return to this discussion below.

4. Monte Carlo simulations

Up to this point, the results we have presented were obtained directly from matrix elements. To give a more realistic assessment of the prospects to observe any of these spin effects in a collider experiment, complete hadron-level events must be considered. We do this using a Monte Carlo (MC) approach. The framework is again the 2HDM (II) because of its special status as the minimal Higgs model compatible with supersymmetry.

The production of $t\bar{t}$ is treated completely within the SM. On the decay end, we study in parallel the situations when either both decays occur within the SM, or when one of the two top quarks decays through $W^{\pm}$ and the other through $H^{\pm}$.[3] Being an interesting process in its own right, the SM decay of $t\bar{t}$ is also the main irreducible background in searches for light $H^{\pm}$ [14]. Over nearly the full range of $\tan\beta$, $H^{\pm}$ decays preferentially to the heaviest lepton available, that is $H^+ \rightarrow \tau^+\nu_\tau$. We therefore restrict ourselves to this decay channel. Consequently, for the SM events, we demand one of the two W bosons to decay through this mode which has $\mathcal{BR}(W^{\pm} \rightarrow \tau^{\pm}\nu_\tau) = 0.1125 \pm 0.0020$. The τ lepton subsequently decays hadronically producing a τ jet. For the other W, which is always present in the event, we consider the hadronic decay to allow for hadronic top reconstruction. We show SM and 2HDM results separately, keeping in mind that $\mathcal{BR}(t \rightarrow bH^+, H^+ \rightarrow \tau^+\nu_\tau)$ and $\mathcal{BR}(t \rightarrow bW^+, W^+ \rightarrow \tau^+\nu_\tau)$ are of similar magnitude for the $\tan\beta$ and m_{H^+} regions of interest.

To incorporate helicity information throughout the whole process, it is necessary to use a MC generator which can treat the full $2 \rightarrow 6$ matrix element. This is provided by MadGraph/MadEvent 4.1.10 [63] for which we implemented the model (3.2). Using this program has the additional advantage that the ME is generated without using the narrow width approximation. To verify the treatment of spin information, control samples were generated using the specialized $t\bar{t}$ generator TopReX 4.11 [64]. For the observables we analyze, results from both programs were found to be in good agreement (after correcting the partial width $\Gamma(t \rightarrow bH^+)$ in TopReX).

From the $2 \rightarrow 6$ matrix element generated by MadEvent, full events are obtained by applying Pythia 6.409 [65] for parton showering and hadronization. To treat properly the spin information in tau decays, which was previously demonstrated to be important in $H^{\pm}$ searches [66, 67], Tauola [68] is invoked. The underlying event is modeled using the Pythia default "old" model based on multiple parton-parton interactions. The default parameters of this model are tuned to Tevatron minimum-bias data [69] and provide reasonable estimates for extrapolation to the LHC energy.

4.1 Event reconstruction

For jet reconstruction we use the FastJet implementation [70] of the longitudinally invariant $k_\perp$ algorithm [71–73] for hadron colliders. The jet clustering uses E-scheme recombination based on the distance measure $d_{ij} = \min(k_{\perp i}^2, k_{\perp j}^2)\Delta R_{ij}^2/R^2$, with $\Delta R = \sqrt{(\Delta\eta)^2 + (\Delta\phi)^2}$

---

[3]Of course, there is also the possibility of having both tops in an event decay through $H^{\pm}$. However, since this mode gives a different final state, and since the effect is sub-leading, we neglect this contribution here.

Model		Number of events		
		Generated	Reconstructed	$\int \mathcal{L}$ (fb^{-1})
SM		804 926	46 524	11.7
$t\bar{t}$ uncorr.		937 552	54 280	13.7
2HDM (II)	$\tan\beta = 50$, $m_{H^+} = 80\,\text{GeV}$	925 806	59 061	3.84
2HDM (II)	$\tan\beta = 1$, $m_{H^+} = 80\,\text{GeV}$	926 690	59 068	7.77

Table 3: Number of events generated at MC level, and events left after reconstruction. Integrated luminosities, corresponding to the generated event samples, are calculated using the NLO $t\bar{t}$ cross section. The luminosity varies due to the different branching ratios for the final state $\tau\nu_\tau jj$.

and $R^2 = 1$. We use the algorithm in *exclusive* mode, meaning that particles are clustered with the beam when the beam-particle distance d_{iB} is smaller than the distance d_{ij} to any jet candidate. Not all particles will therefore end up in a jet. Furthermore, we only take particles with $|\eta| \leq 5$ into account to reflect the detector acceptance region. For the minimum jet separation measure, above which no further clustering takes place, the value $d_{\text{cut}} = 400$ (GeV)^2 is used. Choosing this value gives a jet multiplicity which peaks at the value expected from the matrix element.

We also implement a simplistic notion of flavor tagging where jets are tagged as b jets or τ jets by comparing to MC truth information. A candidate jet is tagged whenever the distance ΔR to a true b quark (or a τ) is less than 0.4. In addition, for the jet to be tagged, it is required that it has $|\eta| \leq 2.5$. Apart from these criteria, no further efficiency factor is used in the flavor tagging.

Events are selected for analysis based on their overall topology. The characteristic signature, which must be fulfilled by our signal events following jet reconstruction, is the presence of exactly two b jets, one τ jet and at least two additional, untagged, jets. For this type of potential $t\bar{t}$ events, the hadronically decaying W is reconstructed by combining two light jets, minimizing the mass-square difference $\Delta m_W^2 = (m_{jj} - m_W)^2$. For W candidates within a certain mass range $\Delta m_W \leq 10\,\text{GeV}$ of the true W mass, further recombination with one of two b jets is performed to reconstruct a $t(\bar{t})$ candidate. On this candidate, a similar cut as for the W on $\Delta m_t^2 = (m_{jjb} - m_t)^2$ is applied to asses the overall goodness of the reconstruction. We keep events which have $\Delta m_t < 15\,\text{GeV}$. For the surviving events, one side has then been fully reconstructed. The remaining b jet, not used in the top reconstruction, can therefore be associated with the $t \to bH^\pm/W^\pm \to b\tau^\pm\nu_\tau$ decay.

To show the statistical efficiency, we give in table 3 the total number of MC events generated for each model. Since the branching ratios to reach the requested final state are largely different for the SM and the 2HDM, this nearly constant number of events actually corresponds to quite different integrated luminosities, as also given in the table. Note that, for these low Higgs masses, the luminosity corresponding to this number of events is highest for the SM sample. Table 3 also lists the total number of events left in each

case after reconstruction. These numbers indicate the level of statistical uncertainty in the jet-level distributions we show below.

Due to the presence of at least *two* neutrinos in the final state from the decay of the $H^{\pm}$ (or $W^{\pm}$) into $\tau^{\pm}\nu_\tau$, the longitudinal momentum of the $t(\bar{t})$ on that side of the event cannot be reconstructed. Thus its rest system is not accessible, neither is the overall CM frame. This fact effectively prevents the direct experimental use of distributions such as (3.16) or (3.17) to establish the presence of a $t \to bH^+$ channel. This is in contrast to the SM case where the semi-leptonic channels involving an e or a μ could be very useful in establishing the existence of $t\bar{t}$ spin correlations. In the following sections, we will focus on how to address this somewhat discouraging situation.

4.2 Distributions in $\Delta\phi$

We will first investigate if there are interesting observables defined directly in the laboratory frame. An early study [19] established that distributions in azimuthal angle $\Delta\phi(l^+l^-)$, with the l^+l^- originating from two leptonic decays of a $t\bar{t}$ pair, are sensitive to $t\bar{t}$ spin correlations. These results were recently confirmed in a NLO shower MC study [30], where also other spin-sensitive observables defined directly from lab quantities were considered. Their conclusion was that, for all the variables included in the study (see [30] for the complete list), the spin effects are only visible in the distribution $\Delta\phi(l^+l^-)$.

Since we require hadronic reconstruction of a W boson and a top quark, we are effectively limited to studying the two distributions $\Delta\phi(b\bar{b})$ and $\Delta\phi(\tau\bar{b})$. From what we know about the spin analyzing efficiencies, we expect, at least for the Higgs case, that these variables could show some effects which were not visible in the SM study. The resulting azimuthal distributions are shown in figure 11. In addition to showing the SM and the 2HDM (II) for $\tan\beta = 50$, and $\tan\beta = 1$, we show also this time the SM *without* any spin correlations to illustrate that this distribution is not a flat line. From the $\Delta\phi(b\bar{b})$ distribution, it can be seen again that the low $\tan\beta$ case is more SM-like and that the high $\tan\beta$ case gives the most significant deviation from the SM distribution. In the $\Delta\phi(\tau\bar{b})$ distribution, the curves are hardly separable. It therefore remains to be seen if these variables could be used in any way to discriminate between the SM and new physics contributions.

Finally we note that these distributions are quite sensitive to changes in the Higgs mass. Larger values of $\Delta\phi$ are favored with increasing m_{H^+}. The kinematic effects must therefore be under good control if the $\Delta\phi$ distributions should be used to determine $\tan\beta$.

4.3 Brandenburg observables

We now turn our attention from the laboratory frame observables to what can be done with half the event fully reconstructed. This has been discussed by Brandenburg who introduced [26] the observables

$$\begin{aligned}
\mathcal{O}_1 &= \mathbf{k}_1^* \cdot \tilde{\mathbf{k}}_2 \\
\mathcal{O}_2 &= (\mathbf{k}_1^* \cdot \hat{\mathbf{z}})(\tilde{\mathbf{k}}_2 \cdot \hat{\mathbf{z}}) \\
\mathcal{O}_3 &= (\mathbf{k}_1^* \cdot \mathbf{p})(\tilde{\mathbf{k}}_2 \cdot \mathbf{p}),
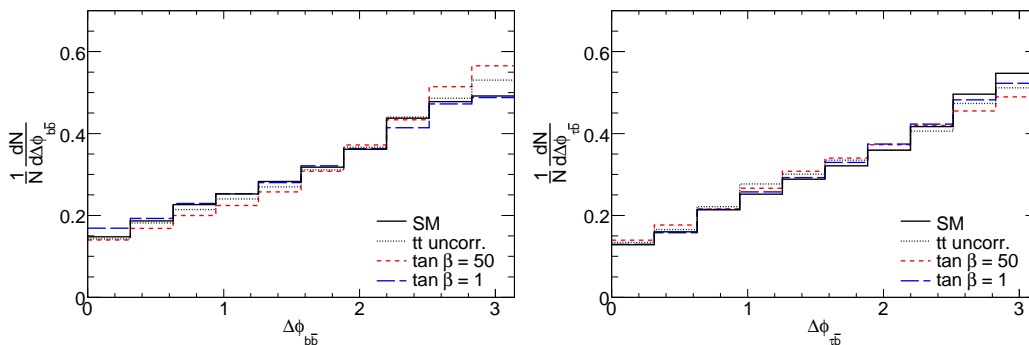\end{aligned} \tag{4.1}$$

Figure 11: Azimuthal angle between b jet from W decay and opposite side b- or τ jet. The results are shown for the SM $t\bar{t}$ (black), or $t \rightarrow bH^+$ decay with $\tan\beta = 50$ (short-dashed red) and $\tan\beta = 1$ (long-dashed blue). For comparison, the distribution obtained in the SM without spin correlations is shown as a dotted black line. The mass $m_{H^+} = 80\,\mathrm{GeV}$ was used.

Model		Observable		
		$\langle \mathcal{O}_1 \rangle$	$\langle \mathcal{O}_2 \rangle$	$\langle \mathcal{O}_3 \rangle$
SM		-2.08	-0.25	-0.67	%
2HDM (II)	$\tan\beta = 1$	-1.06	-0.11	-0.31	%
2HDM (II)	$\tan\beta = 50$	0.86	0.04	0.24	%

Table 4: Mean value of the Brandenburg observables in percent. Evaluated for SM ($W^\pm W^\mp$) and charged Higgs ($W^\pm H^\mp$) decay of $t\bar{t}$ with $m_{H^+} = 80\,\mathrm{GeV}$.

where an asterisk denotes momenta in the rest frame of the parent top quark. The beam direction is given by $\hat{\mathbf{z}}$, and $\tilde{\mathbf{k}}_2$ is the laboratory momentum of the lepton from the top decay not associated with $\mathbf{k}_1$. Each of the observables $\mathcal{O}_1 - \mathcal{O}_3$ are cleverly constructed to have mean value strictly equal to zero in the absence of $t\bar{t}$ spin correlations. We first evaluated $\mathcal{O}_1 - \mathcal{O}_3$ at parton-level, similarly to what is done in [26], but also including the decay through $H^\pm$. The resulting mean values obtained from the distributions in these observables are presented in table 4. Their standard deviations are $\Delta\mathcal{O}_1 = 0.58$, $\Delta\mathcal{O}_2 = 0.42$ and $\Delta\mathcal{O}_3 = 0.39$ for all three cases. Comparing our SM values with those given in the original study, we find that there is an overall agreement. For the Higgs case, we observe the same sign differences between the low and high $\tan\beta$ regimes as previously seen for the correlation plots. We also note that the Higgs values are generally smaller than their SM counterparts.

Unfortunately, when evaluated at the jet level, including the cuts described above, we find that the expectation values for all three Brandenburg observables are consistent with zero.
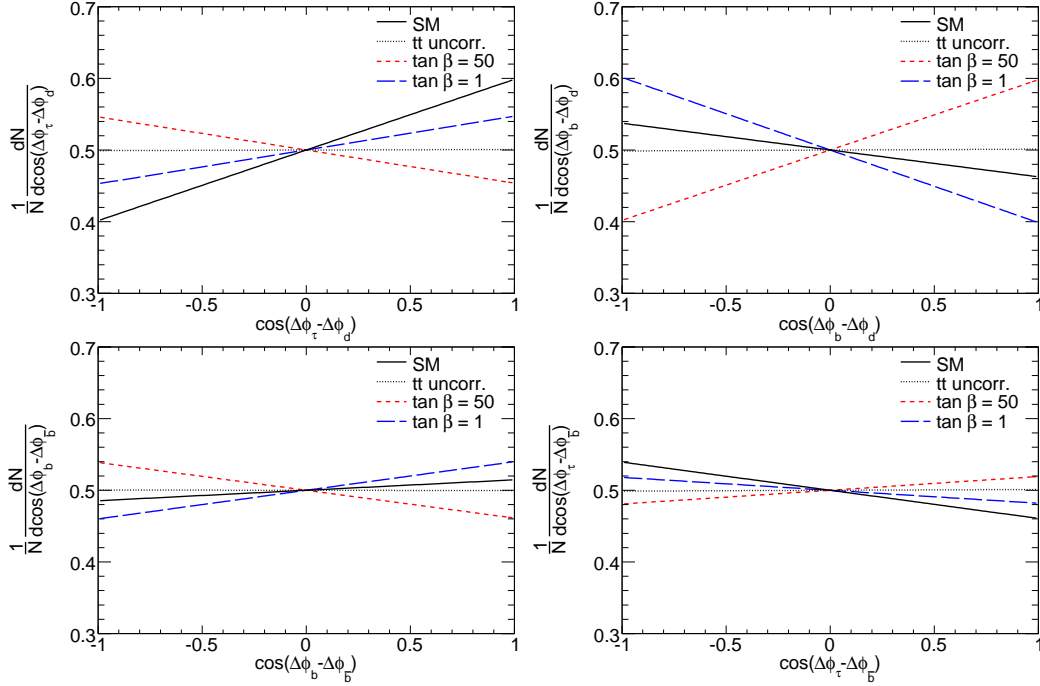
Figure 12: Distributions at matrix element level of $\cos(\Delta\phi_i - \Delta\phi_j)$ for different final state particles (i,j). Dotted line show results in the SM *without* spin correlations. SM results with correlations are shown in solid black. The 2HDM (II) is shown for $\tan\beta = 1$ (dashed blue), and $\tan\beta = 50$ (dotted red). All results were obtained for $m_{H^+} = 80\,\text{GeV}$.

4.4 Transverse correlations

As an alternative to the full reconstruction of the rest frames for t and $\bar{t}$, and the half reconstruction performed when calculating the Brandenburg observables, we consider transverse reconstruction. This is possible in the hadronic channel where one top quark is reconstructed using the methods discussed above, while the transverse momentum of the other top can be obtained from the sum $p_{\perp,t} = p_{\perp,b} + p_{\perp,\tau} + p_{\perp,\text{miss}}$. The sum involves the b jet not used for top reconstruction in the first step.

Following the reconstruction, we perform boosts of particles (i,j) into the *transverse* rest frames of $t(\bar{t})$, and consider distributions in this frame of azimuthal angles $(\Delta\phi_i, \Delta\phi_j)$ to the $p_\perp$ axes of $t(\bar{t})$. It is then possible to form both doubly differential distributions similar to (3.16), or one-dimensional distributions similar to (3.17). To obtain a distribution which like (3.17) is robust with respect to cuts, we have looked specifically at distributions in $\Delta\phi_i - \Delta\phi_j$. In analogy with the construction of CM variables, we expect a distribution of the form

$$\frac{1}{N}\frac{\mathrm{d}N}{\mathrm{d}\cos(\Delta\phi_i - \Delta\phi_j)} = \frac{1}{2}\Big[1 + \mathcal{D}'\alpha_i\alpha_j\cos(\Delta\phi_i - \Delta\phi_j)\Big]. \tag{4.2}$$

This relation involves yet another spin correlation coefficient $\mathcal{D}'$. To illustrate how similar this new observable is to $\cos\theta_{ij}$, which was previously shown in figure 10, figure 12 shows the matrix element results on $\cos(\Delta\phi_i - \Delta\phi_j)$ for the same particle combinations. The

results are presented for the SM, and for the charged Higgs decay with $\tan\beta = 50$ and $\tan\beta = 1$. From comparing the two figures, we note that $\mathcal{D}' \simeq 0.9\mathcal{D}$, signaling only a slight loss of correlation going to the transverse projection.

These transverse correlations also maintain their properties when going to the level of jets, as demonstrated in figure 13. That only two diagrams are shown in figure 13, and not even the ones from figure 12 with best separation between the different cases, is because the efficiency in experimentally separating a d-type jet from a u-type jet is only 61% [23]. Since this separation step is required in order to use the jets from the hadronic W decay in the analysis, we exclude the (τ, d) and (b, d) combinations, which both require this information. We remind the reader that the distribution $(H^+, \bar{b})$ contains the same information as that for $(b, \bar{b})$. This is true also at jet level, since the momenta of H^+ and b are still anti-parallel in the reconstructed top rest frame. Figure 13 shows good separation between the SM and the 2HDM (II) for $\tan\beta = 50$, while the small $\tan\beta$ case is more difficult to separate from the SM. Since this small separation is partly intrinsic, as can be seen from the lower panels in figure 12, these variables show most promise in the high $\tan\beta$ regime.

We have studied the dependence of the distributions in figure 13 on m_{H^+}. From their α dependence, the coupling sensitivity in the $(\tau, \bar{b})$ correlation is expected to degrade for higher m_{H^+}, while it should not change for $(b, \bar{b})$. This is indeed what is observed. We also find additional distortion in both distributions when $m_{H^+} \gtrsim 130\,\text{GeV}$. For $(b, \bar{b})$, values $\cos(\Delta\phi_b - \Delta\phi_{\bar{b}}) < 0$ are favored, while for the $(\tau, \bar{b})$ distribution instead $\cos(\Delta\phi_\tau - \Delta\phi_{\bar{b}}) > 0$ shows a surplus of events. However, due to the small values of α_τ for $H^\pm$, the $(\tau, \bar{b})$ distribution is hardly interesting for such masses. This additional angular dependence, which is not observed at parton level, we attribute to the b jet reconstruction. For higher m_{H^+}, the b quarks from $t \to bH^+$ become softer, and eventually fall below the jet measure d_{cut} in $p_\perp$. These events should normally not pass for further analysis, if not the underlying event provided the necessary energy. When these jets are dominated by the underlying event, their directions are smeared, causing the t rest frame to be poorly reconstructed. The result is an additional distortion in the angular distributions compared to the ME results.

5. Summary and conclusions

Top quarks produced in pairs at the LHC should experience strong correlations between their spin projections in the helicity basis. This entanglement makes it a favorable system for studying the Lorentz structure of the couplings involved in top quark production and decay. We have considered here the effects on spin dependent angular observables of new physics in top quark decays. Specifically, we have discussed top decay through a charged Higgs boson.

Within a general CP-conserving 2HDM, we obtain results on the spin analyzing coefficients. They determine the sensitivity of a given decay product to the spin projection of the decaying particle. Unlike the SM decay $t \to bW^+ \to bl^+\nu_l$, where the charged lepton (or d quark jet) is the most powerful spin analyzer, the scalar case has the associated b
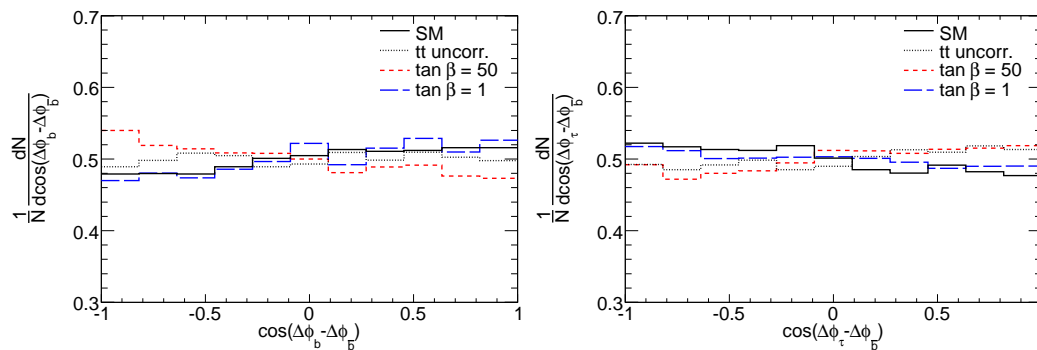
Figure 13: Distributions at jet level of $\cos(\Delta\phi_i - \Delta\phi_j)$ for different final state particles (i, j). The different contours correspond to the SM with (solid black), and without (black dotted), $t\bar{t}$ spin correlations. There is also the 2HDM (II) for $\tan\beta = 1$ (dashed blue), and for $\tan\beta = 50$ (dotted red). All results were obtained for $m_{H^+} = 80\,\mathrm{GeV}$.

quark, or the $H^{\pm}$ momentum itself, as the most efficient spin analyzers. As for the lepton in the SM case, this efficiency can reach unity. In the 2HDM (II), this is found to be the case for very large (and very small) values of $\tan\beta$. At the level of matrix elements, the modification to the distributions of certain angular observables, induced by the presence of an $H^{\pm}$, could therefore be similar in magnitude to the SM spin effects themselves. Whether this is actually the case depends on the parameters of the 2HDM. Since all spin analyzing coefficients associated with $t \to bH^{\pm} \to b\tau^{\pm}\nu_\tau$ depend universally on the Lorentz structure of the tbH^+ vertex, an angular analysis of the decay products could provide an additional handle on the $H^{\pm}$ couplings. This includes the possibility of determining the effective value of $\tan\beta$ in the MSSM, since we find that $\tan\beta$ enhanced SUSY corrections to the spin correlation observables are small.

The preference of the $H^{\pm}$ to decay into $\tau^{\pm}\nu_\tau$ prevents reconstruction of longitudinal momenta. Thus the $t(\bar{t})$ rest frame spin analysis, which can be performed in the SM, cannot be directly applied to the new physics case. Encouraged by the significant spin effects observed at matrix element level, we have therefore studied several longitudinally boost-invariant observables.

We find that the distribution in azimuthal angle between the b jet associated with $t \to bH^+$, and the b jet from the opposite side $t \to bW$ decay, shows some sensitivity to the Lorentz structure of the $H^{\pm}$ coupling. Although the effects on this observable are small, they are directly measurable and therefore shows promise for further experimental study.

Even more promising are $(\Delta\phi_i, \Delta\phi_j)$ correlations in the transverse rest frames of $t(\bar{t})$. This observable is also directly measurable, and it is found to be robust with respect to phase-space cuts. The highest sensitivity is also here obtained for the $(b, \bar{b})$ correlation. This distribution should be particularly useful in the highly interesting case with large $\tan\beta$, as it lifts the degeneracy between large and small $\tan\beta$ values present in the inclusive $\mathcal{BR}(t \to bH^+)$ measurement. It should be investigated if this observable could be useful also for studying $t\bar{t}$ spin effects within the SM. In that case, it should be possible to use

(l, b) distributions where $l = e, \mu$. Another question is if the correlations in $(b, \bar{b})$ or (l, b) obtained from the semi-leptonic $t\bar{t}$ decay in the SM could be used as control samples.

As illustrated by our MC samples, statistics is not the limiting factor in an analysis of this type due to the large cross section for $t\bar{t}$ production at the LHC. We therefore conclude that further investigation of spin effects in top physics beyond the Standard Model should be worthwhile.

Acknowledgments

A. Massive spinor formalism

In this appendix, we discuss the formalism used to describe polarized massive fermions. Throughout the discussion, we try to adhere to the conventions of [74] which contains an excellent introduction to spin formalism.

For massive spin-1/2 particles, the projection relations

$$
\begin{aligned}
\sum_{\lambda=\pm\frac{1}{2}} u(p, \lambda)\bar{u}(p, \lambda) &= \slashed{p} + m \\
\sum_{\lambda=\pm\frac{1}{2}} v(p, \lambda)\bar{v}(p, \lambda) &= \slashed{p} - m
\end{aligned}
\tag{A.1}
$$

obtained by summing over the possible helicity states λ are very well-known, as are the more general projector relations

$$
\begin{aligned}
u(p, \lambda)\bar{u}(p, \lambda) &= \frac{1}{2}\left(1 + \gamma_5\slashed{s}\right)\left(\slashed{p} + m\right) \\
v(p, \lambda)\bar{v}(p, \lambda) &= \frac{1}{2}\left(1 + \gamma_5\slashed{s}\right)\left(\slashed{p} - m\right)
\end{aligned}
\tag{A.2}
$$

with a time-like spin four-vector defined as

$$
s^\mu = 2\lambda\left(\frac{|\mathbf{p}|}{m}, \frac{E}{m}\hat{\mathbf{p}}\right).
\tag{A.3}
$$

In the rest frame of the massive particle $s^\mu = 2\lambda(0, \hat{\mathbf{p}})$, whereas in the high-energy limit $s^\mu = 2\lambda p^\mu/m$. As a further generalization of the projector technique, Bouchiat and Michel [75] introduced a projection relation for the more general product of two Dirac spinors of mass m with arbitrary helicities. For this we need to introduce three spin vectors s_μ^a that are mutually orthonormal, and in addition orthogonal to p/m in the sense:

$$
\begin{aligned}
p \cdot s^a &= 0 \\
s^a \cdot s^b &= -\delta^{ab} \\
s_\mu^a s_\nu^a &= -g_{\mu\nu} + \frac{p_\mu p_\nu}{m^2}.
\end{aligned}
\tag{A.4}
$$

The most direct choice for an explicit spin basis of this type is perhaps, in a coordinate system where $\hat{\mathbf{p}}$ is in the positive z-direction, to use

$$\begin{aligned}
s^{1\mu} &= (0, \hat{\mathbf{x}}) \\
s^{2\mu} &= (0, \hat{\mathbf{y}}) \\
s^{3\mu} &= \left(\frac{|\mathbf{p}|}{m}, \frac{E}{m}\hat{\mathbf{p}}\right).
\end{aligned} \tag{A.5}$$

With this choice, $s^{3\mu}$ differs from the positive helicity spin vector (A.3) only by a factor 2λ. The helicity spinors can be shown to satisfy

$$\begin{aligned}
\gamma_5 \slashed{s}^a u(p, \lambda') &= \sigma^a_{\lambda\lambda'} u(p, \lambda) \\
\gamma_5 \slashed{s}^a v(p, \lambda') &= \sigma^a_{\lambda'\lambda} v(p, \lambda)
\end{aligned} \tag{A.6}$$

where the rhs is summed over λ, and the σ^a are Pauli matrices where the first (second) row and column correspond to $\lambda = 1/2$ ($\lambda = -1/2$). Thus $\sigma^3 = 2\lambda I$. From these identities, the Bouchiat-Michel relations

$$\begin{aligned}
u(p, \lambda')\bar{u}(p, \lambda) &= \frac{1}{2}\left(\delta_{\lambda\lambda'} + \gamma^5 \slashed{s}^a \sigma^a_{\lambda\lambda'}\right)(\slashed{p} + m) \\
v(p, \lambda')\bar{v}(p, \lambda) &= \frac{1}{2}\left(\delta_{\lambda\lambda'} + \gamma^5 \slashed{s}^a \sigma^a_{\lambda'\lambda}\right)(\slashed{p} - m).
\end{aligned} \tag{A.7}$$

follow. Letting $\lambda' = \lambda$ (no sum over λ), and noting that $s^i_{\lambda\lambda} \neq 0$ only for $i = 3$ with the spin basis (A.5), the relations (A.2) are obtained as a special case of the Bouchiat-Michel formulae.

References

[1] R.M. Barnett, H.E. Haber and D.E. Soper, *Ultraheavy particle production from heavy partons at hadron colliders*, *Nucl. Phys.* **B 306** (1988) 697.

[2] A.C. Bawa, C.S. Kim and A.D. Martin, *Charged Higgs production at hadron colliders*, *Z. Physik* **C 47** (1990) 75.

[3] F. Borzumati, J.-L. Kneur and N. Polonsky, *Higgs-strahlung and R-parity violating slepton-strahlung at hadron colliders*, *Phys. Rev.* **D 60** (1999) 115011 [hep-ph/9905443].

[4] D.J. Miller, S. Moretti, D.P. Roy and W.J. Stirling, *Detecting heavy charged Higgs bosons at the LHC with four B quark tags*, *Phys. Rev.* **D 61** (2000) 055011 [hep-ph/9906230].

[5] S.L. Glashow and E.E. Jenkins, *A light top quark after all?*, *Phys. Lett.* **B 196** (1987) 233.

[6] V.D. Barger and R.J.N. Phillips, *Bounds on a top quark with charged Higgs decay*, *Phys. Lett.* **B 201** (1988) 553.

[7] V.D. Barger and R.J.N. Phillips, *Signals of top quarks with charged Higgs decay at $p\bar{p}$ colliders*, *Phys. Rev.* **D 40** (1989) 2875.

[8] V.D. Barger and R.J.N. Phillips, *Hidden top quark with charged Higgs decay*, *Phys. Rev.* **D 41** (1990) 884.

[9] R.M. Godbole and D.P. Roy, *Charged Higgs search via heavy top decay at Tevatron collider energy*, *Phys. Rev.* **D 43** (1991) 3640.

[10] ALEPH collaboration, A. Heister et al., *Search for charged Higgs bosons in e^+e^- collisions at energies up to $\sqrt{s} = 209\,GeV$*, *Phys. Lett.* **B 543** (2002) 1 [hep-ex/0207054].

[11] CDF collaboration, A. Abulencia et al., *Search for charged Higgs bosons from top quark decays in $p\bar{p}$ collisions at $\sqrt{s} = 1.96\,TeV$*, *Phys. Rev. Lett.* **96** (2006) 042003 [hep-ex/0510065].

[12] D. Denegri et al., *Summary of the cms discovery potential for the MSSM SUSY higgses*, hep-ph/0112045.

[13] K.A. Assamagan, Y. Coadou and A. Deandrea, *ATLAS discovery potential for a heavy charged Higgs boson*, *Eur. Phys. J.* **C 4** (2002) 9 [hep-ph/0203121].

[14] C. Biscarat and M. Dosil, *Charged Higgs search in top quark decays with the ATLAS detector*, ATL-PHYS-2003-038.

[15] M. Baarmand, M. Hashemi and A. Nikitenko, *Light charged Higgs discovery potential of CMS in the $H^+ \to \tau\nu_\tau$ decay with single lepton trigger*, *J. Phys.* **G 32** (2006) 21.

[16] B. Mohn, M. Flechl and J. Alwall, *ATLAS discovery potential for the charged Higgs boson in $H^+ \to \tau\nu_\tau$ decays*, ATL-PHYS-PUB-2007-006.

[17] I.I.Y. Bigi, Y.L. Dokshitzer, V.A. Khoze, J.H. Kuhn and P.M. Zerwas, *Production and decay properties of ultraheavy quarks*, *Phys. Lett.* **B 181** (1986) 157.

[18] J.H. Kuhn, *How to measure the polarization of top quarks*, *Nucl. Phys.* **B 237** (1984) 77.

[19] V.D. Barger, J. Ohnemus and R.J.N. Phillips, *Spin correlation effects in the hadroproduction and decay of very heavy top quark pairs*, *Int. J. Mod. Phys.* **A 4** (1989) 617.

[20] Y. Hara, *Angular correlation of charged leptons from $t\bar{t}$ produced in the gluon fusion*, *Prog. Theor. Phys.* **86** (1991) 779.

[21] T. Arens and L.M. Sehgal, *Azimuthal correlation of charged leptons produced in $p\bar{p} \to t\bar{t}$*, *Phys. Lett.* **B 302** (1993) 501.

[22] D. Chang, S.-C. Lee and P. Turcotte, *The interference effect of top quark polarization at hadronic colliders*, *Chin. J. Phys.* **34** (1996) 748 [hep-ph/9508357].

[23] G. Mahlon and S.J. Parke, *Angular correlations in top quark pair production and decay at hadron colliders*, *Phys. Rev.* **D 53** (1996) 4886 [hep-ph/9512264].

[24] T. Stelzer and S. Willenbrock, *Spin correlation in top-quark production at hadron colliders*, *Phys. Lett.* **B 374** (1996) 169 [hep-ph/9512292].

[25] D. Chang, S.-C. Lee and A. Sumarokov, *On the observation of top spin correlation effect at Tevatron*, *Phys. Rev. Lett.* **77** (1996) 1218 [hep-ph/9512417].

[26] A. Brandenburg, *Spin-spin correlations of top quark pairs at hadron colliders*, *Phys. Lett.* **B 388** (1996) 626 [hep-ph/9603333].

[27] G. Mahlon and S.J. Parke, *Maximizing spin correlations in top quark pair production at the Tevatron*, *Phys. Lett.* **B 411** (1997) 173 [hep-ph/9706304].

[28] W. Bernreuther, A. Brandenburg, Z.G. Si and P. Uwer, *Top quark spin correlations at hadron colliders: predictions at next-to-leading order QCD*, *Phys. Rev. Lett.* **87** (2001) 242002 [hep-ph/0107086].

[29] W. Bernreuther, A. Brandenburg, Z.G. Si and P. Uwer, *Top quark pair production and decay at hadron colliders*, *Nucl. Phys.* **B 690** (2004) 81 [`hep-ph/0403035`].

[30] S. Frixione, E. Laenen, P. Motylinski and B.R. Webber, *Angular correlations of lepton pairs from vector boson and top quark decays in Monte Carlo simulations*, *JHEP* **04** (2007) 081 [`hep-ph/0702198`].

[31] G.L. Kane, G.A. Ladinsky and C.P. Yuan, *Using the top quark for testing standard model polarization and CP predictions*, *Phys. Rev.* **D 45** (1992) 124.

[32] T. Arens and L.M. Sehgal, *Secondary leptons as probes of top quark polarization in $e^+e^- \to t\bar{t}$*, *Nucl. Phys.* **B 393** (1993) 46.

[33] C.R. Schmidt, *Top quark production and decay at next-to-leading order in e^+e^- annihilation*, *Phys. Rev.* **D 54** (1996) 3250 [`hep-ph/9504434`].

[34] S.J. Parke and Y. Shadmi, *Spin correlations in top quark pair production at e^+e^- colliders*, *Phys. Lett.* **B 387** (1996) 199 [`hep-ph/9606419`].

[35] A. Brandenburg, M. Flesch and P. Uwer, *The spin density matrix of top quark pairs produced in electron positron annihilation including QCD radiative corrections*, *Phys. Rev.* **D 59** (1999) 014001 [`hep-ph/9806306`].

[36] H.X. Liu, C.S. Li and Z.J. Xiao, *$O(\alpha_s)$ QCD corrections to spin correlations in $e^-e^+ \to t\bar{T}$ process at the NLC*, *Phys. Lett.* **B 458** (1999) 393 [`hep-ph/9901205`].

[37] F. del Aguila and J.A. Aguilar-Saavedra, *Precise determination of the Wtb couplings at LHC*, *Phys. Rev.* **D 67** (2003) 014009 [`hep-ph/0208171`].

[38] J.A. Aguilar-Saavedra, J. Carvalho, N. Castro, F. Veloso and A. Onofre, *Probing anomalous Wtb couplings in top pair decays*, *Eur. Phys. J.* **C 50** (2007) 519 [`hep-ph/0605190`].

[39] C.R. Schmidt and M.E. Peskin, *A probe of CP-violation in top quark pair production at hadron supercolliders*, *Phys. Rev. Lett.* **69** (1992) 410.

[40] W. Bernreuther, O. Nachtmann, P. Overmann and T. Schroder, *Angular correlations and distributions for searches of CP-violation in top quark production and decay*, *Nucl. Phys.* **B 388** (1992) 53.

[41] A. Brandenburg and J.P. Ma, *CP odd observables for the top-anti-top system produced at proton-anti-proton and proton proton colliders*, *Phys. Lett.* **B 298** (1993) 211.

[42] W. Bernreuther and A. Brandenburg, *Signatures of Higgs sector CP-violation in top quark pair production at proton proton supercolliders*, *Phys. Lett.* **B 314** (1993) 104.

[43] W. Bernreuther and A. Brandenburg, *Tracing CP-violation in the production of top quark pairs by multiple TeV proton proton collisions*, *Phys. Rev.* **D 49** (1994) 4481 [`hep-ph/9312210`].

[44] J.G. Korner and M.C. Mauser, *$O(\alpha_s)$ radiative corrections to polarized top decay into a charged Higgs $t(\text{pol.}) \to H^+ + b$*, `hep-ph/0211098`.

[45] M. Arai, N. Okada, K. Smolek and V. Simak, *Top spin correlations in theories with large extra-dimensions at the Large Hadron Collider*, *Phys. Rev.* **D 70** (2004) 115015 [`hep-ph/0409273`].

[46] M. Arai, N. Okada, K. Smolek and V. Simak, *Top quark spin correlations in the Randall-Sundrum model at the CERN Large Hadron Collider*, *Phys. Rev.* **D 75** (2007) 095008 [`hep-ph/0701155`].

[47] CDF collaboration, *A combination of CDF and D0 results on the mass of the top quark*, `hep-ex/0703034`.

[48] P. Nason, S. Dawson and R.K. Ellis, *The total cross-section for the production of heavy quarks in hadronic collisions*, *Nucl. Phys.* **B 303** (1988) 607.

[49] P. Nason, S. Dawson and R.K. Ellis, *The one particle inclusive differential cross-section for heavy quark production in hadronic collisions*, *Nucl. Phys.* **B 327** (1989) 49.

[50] J. Pumplin et al., *New generation of parton distributions with uncertainties from global QCD analysis*, *JHEP* **07** (2002) 012 [`hep-ph/0201195`].

[51] S. Frixione, P. Nason and G. Ridolfi, *A positive-weight next-to-leading-order Monte Carlo for heavy flavour hadroproduction*, *JHEP* **09** (2007) 126 [`arXiv:0707.3088`].

[52] M.S. Carena, D. Garcia, U. Nierste and C.E.M. Wagner, *Effective lagrangian for the $\bar{t}BH^+$ interaction in the MSSM and charged Higgs phenomenology*, *Nucl. Phys.* **B 577** (2000) 88 [`hep-ph/9912516`].

[53] E. Braaten and J.P. Leveille, *Higgs boson decay and the running mass*, *Phys. Rev.* **D 22** (1980) 715.

[54] M. Drees and K.-i. Hikasa, *Note on QCD corrections to hadronic Higgs decay*, *Phys. Lett.* **B 240** (1990) 455.

[55] G. Degrassi, P. Gambino and G.F. Giudice, *$B \to X_s\gamma$ in supersymmetry: large contributions beyond the leading order*, *JHEP* **12** (2000) 009 [`hep-ph/0009337`].

[56] L.J. Hall, R. Rattazzi and U. Sarid, *The top quark mass in supersymmetric SO(10) unification*, *Phys. Rev.* **D 50** (1994) 7048 [`hep-ph/9306309`].

[57] B. Grzadkowski and W. Hollik, *Radiative corrections to the top quark width within two Higgs doublet models*, *Nucl. Phys.* **B 384** (1992) 101.

[58] J.-j. Cao, R.J. Oakes, F. Wang and J.M. Yang, *Supersymmetric effects in top quark decay into polarized W-boson*, *Phys. Rev.* **D 68** (2003) 054019 [`hep-ph/0306278`].

[59] R. Ellis, W.J. Stirling and B.R. Webber, *QCD and collider physics*, Cambridge University Press, Cambridge U.K. (1996).

[60] M. Jezabek and J.H. Kuhn, *Lepton spectra from heavy quark decay*, *Nucl. Phys.* **B 320** (1989) 20.

[61] A. Czarnecki and M. Jezabek, *Distributions of leptons in decays of polarized heavy quarks*, *Nucl. Phys.* **B 427** (1994) 3 [`hep-ph/9402326`].

[62] A. Czarnecki, M. Jezabek and J.H. Kuhn, *Lepton spectra from decays of polarized top quarks*, *Nucl. Phys.* **B 351** (1991) 70.

[63] J. Alwall et al., *MadGraph/MadEvent v4: the new web generation*, *JHEP* **09** (2007) 028 [`arXiv:0706.2334`].

[64] S.R. Slabospitsky and L. Sonnenschein, *Toprex generator (version 3.25): short manual*, *Comput. Phys. Commun.* **148** (2002) 87 [`hep-ph/0201292`].

[65] T. Sjöstrand, S. Mrenna and P. Skands, *PYTHIA 6.4 physics and manual*, *JHEP* **05** (2006) 026 [`hep-ph/0603175`].

[66] D.P. Roy, *Using τ polarization for the charged Higgs search at hadron colliders*, *Phys. Lett.* **B 277** (1992) 183.

[67] S. Raychaudhuri and D.P. Roy, *Sharpening up the charged Higgs boson signature using tau polarization at LHC*, *Phys. Rev.* **D 53** (1996) 4902 [`hep-ph/9507388`].

[68] S. Jadach, Z. Was, R. Decker and J.H. Kuhn, *The τ decay library TAUOLA: version 2.4*, *Comput. Phys. Commun.* **76** (1993) 361.

[69] CDF collaboration, R. Field and R.C. Group, *PYTHIA tune a, HERWIG and JIMMY in Run 2 at CDF*, `hep-ph/0510198`.

[70] M. Cacciari and G.P. Salam, *Dispelling the N^3 myth for the $k(t)$ jet-finder*, *Phys. Lett.* **B 641** (2006) 57 [`hep-ph/0512210`].

[71] S. Catani, Y.L. Dokshitzer, M.H. Seymour and B.R. Webber, *Longitudinally invariant $k(t)$ clustering algorithms for hadron hadron collisions*, *Nucl. Phys.* **B 406** (1993) 187.

[72] S.D. Ellis and D.E. Soper, *Successive combination jet algorithm for hadron collisions*, *Phys. Rev.* **D 48** (1993) 3160 [`hep-ph/9305266`].

[73] Y.L. Dokshitzer, G.D. Leder, S. Moretti and B.R. Webber, *Better jet clustering algorithms*, *JHEP* **08** (1997) 001 [`hep-ph/9707323`].

[74] H.E. Haber, *Spin formalism and applications to new physics searches*, `hep-ph/9405376`.

[75] C. Bouchiat and L. Michel, *Mesure de la polarisation des electrons relativistes*, *Nucl. Phys.* **5** (1958) 416.